Application of Diffusion Weighted Imaging and Diffusion Tensor Imaging in the Pretreatment and Post-treatment of Brain Tumor

Ranliang Hu, MD[a], Michael J. Hoch, MD[b,*]

KEYWORDS

• ADC • Anisotropy • Brain mapping • Glioma • Neurosurgery • Tractography

KEY POINTS

- Clinical diffusion weighted imaging exploits the random motion of water molecules to generate contrast between normal tissue and disease.
- Diffusion is a valuable sequence in the initial evaluation of intracranial tumors, which can narrow the differential diagnosis and increase diagnostic confidence.
- Noninvasive presurgical mapping of eloquent white matter by diffusion tractography can reduce operative complication rates.
- Interpreting radiologists should understand the common causes of nonvisualized fibers by clinical tractography to better guide surgery.

INTRODUCTION

Diffusion MR imaging is a powerful technique that exploits the diffusion properties of water to generate contrast between normal tissue and pathology. The relative restriction of random water movement (diffusion) in vivo is measured using paired diffusion sensitizing gradients, which causes greater signal loss in diffusing relative to stationary spins. Since its introduction 30 years ago, diffusion MR imaging has transformed the practice of radiology by demonstrating high sensitivity and specificity for ischemic, infectious, toxic-metabolic, and neoplastic conditions.[1] In brain tumor imaging, diffusion MR imaging has been used to assess tumor type and grade, treatment response, and guide surgical intervention.[2–4]

Diffusion weighted imaging (DWI) is the most basic implementation of diffusion MR imaging and assumes a simple but clinically useful model of isotropic gaussian diffusion. DWI is "diffusion weighted" because it is not a true map of diffusion but also contains T2 and other contrasts; therefore, at least one additional set of images with no or little diffusion weighting is also required to calculate the apparent diffusion coefficient (ADC), a semiquantitative measure that relates to the actual diffusion coefficient and removes the contribution of "T2 shine-through."

Diffusion tensor imaging (DTI) expands on DWI by fitting a tensor model of diffusion, taking into account anisotropic diffusion in different directions and enabling calculation of metrics, such as fractional anisotropy (FA) (**Table 1**). Furthermore, DTI has been used to produce models of white matter bundles in the brain, or fiber tractography (FT), which is useful for neurosurgical planning and

[a] Department of Radiology & Imaging Sciences, Emory University, Emory University Hospital, 1364 Clifton Road, BG 20, Atlanta, GA 30322, USA; [b] Department of Radiology, University of Pennsylvania, Hospital of the University of Pennsylvania, 3400 Spruce Street, Suite 130, Philadelphia, PA 19104, USA
* Corresponding author.
E-mail address: Michael.Hoch@pennmedicine.upenn.edu

Radiol Clin N Am 59 (2021) 335–347
https://doi.org/10.1016/j.rcl.2021.01.003

Table 1
Description of diffusion tensor–derived metrics

Metric	Definition	Notes
Axial diffusivity	Diffusion magnitude along the primary orientation of axonal fiber bundles	Largest or principal eigenvalue
Radial diffusivity	Diffusion magnitude perpendicular to the axonal fiber bundles	Average of the two minor eigenvalues
Mean diffusivity	Directionally averaged diffusivity of water in a voxel	Average of all 3 eigenvalues; equals ADC
Fractional anisotropy	Degree of coherent directionality of intravoxel diffusivity	Values from 0 to 1 0 = unrestricted 1 = linear

intraoperative navigation. Although there is much exciting research in this area, a detailed physics review of advanced diffusion methods is beyond the scope of this article. The current clinical applications of diffusion imaging for evaluation of brain tumors is our focus.

DIFFUSION WEIGHTED IMAGING

Pretreatment

DWI is a useful sequence in the initial evaluation of intracranial tumors and tumor-like lesions. Restricted diffusion, as demonstrated by increased DWI signal and correspondingly reduced ADC, is caused by decreased free motion of water molecules, either because of high cellular density (eg, lymphoma and medulloblastoma) or high protein content (eg, epidermoid cyst). When used in conjunction with clinical history and other imaging features, DWI can help narrow the differential diagnosis and increase diagnostic confidence.

Extra-axial masses

Meningiomas are the most commonly encountered extra-axial lesion in clinical practice and can have a variable appearance on DWI. Qualitatively, some meningiomas can have slightly increased signal on DWI compared with the adjacent brain parenchymal. Lower ADC values have been reported to be associated with high-grade (atypical or malignant) meningiomas.[5] Similarly, there are also preliminary reports of using ADC to differentiate between hemangiopericytomas from meningiomas (higher ADC in the former), but further study is needed to confirm these findings.[6]

Dermoid and epidermoid cysts are along the histologic spectrum of ectodermal inclusion cysts and are classified depending on the presence of only epidermal component (epidermoid) or epidermal and dermal appendages (dermoid). Desquamated keratin in epidermoid cysts gives them the characteristic high DWI signal, enabling it to be readily differentiated from similar cystic lesions, such as arachnoid cyst.[7] Dermoid cysts can have variable high DWI signal depending on amount of desquamated keratin, but they also have high T1 signal because of their lipid content. Practically, clear distinction between dermoid and epidermoid at imaging is not crucial, because it does not alter management of these related benign entities.

Intra-axial masses

Diffusion imaging is helpful in the evaluation of pediatric and adult intra-axial tumors. In children, medulloblastomas and other embryonal tumors typically demonstrate high DWI signal and reduced ADC because of their high cellularity and nuclear-to-cytoplasmic ratio. This enables reliable distinction from other posterior fossa masses, such as ependymoma (**Fig. 1**) and pilocytic astrocytoma, which tend to have intermediate or facilitated diffusion.[8] Atypical teratoid/rhabdoid tumor is an aggressive embryonal tumor that also demonstrates restricted diffusion, but typically presents in a younger age group than medulloblastomas (<2 years vs mid to later childhood).

DWI plays a key role in the differentiation of gliomas and lymphomas, two of the most commonly encountered adult brain tumors. Central nervous system lymphoma are usually homogeneously hyperintense on DWI and has significantly lower ADC than glioblastoma, $0.630 \pm 0.155 \times 10^{-3}$ mm^2/s versus $0.963 \pm 0.119 \times 10^{-3}$ mm^2/s.[9] Diffusion within glioma varies from intermediate to high and correlates with histologic grade, with higher-grade tumors, such as anaplastic astrocytomas and glioblastoma, demonstrating lower ADC than

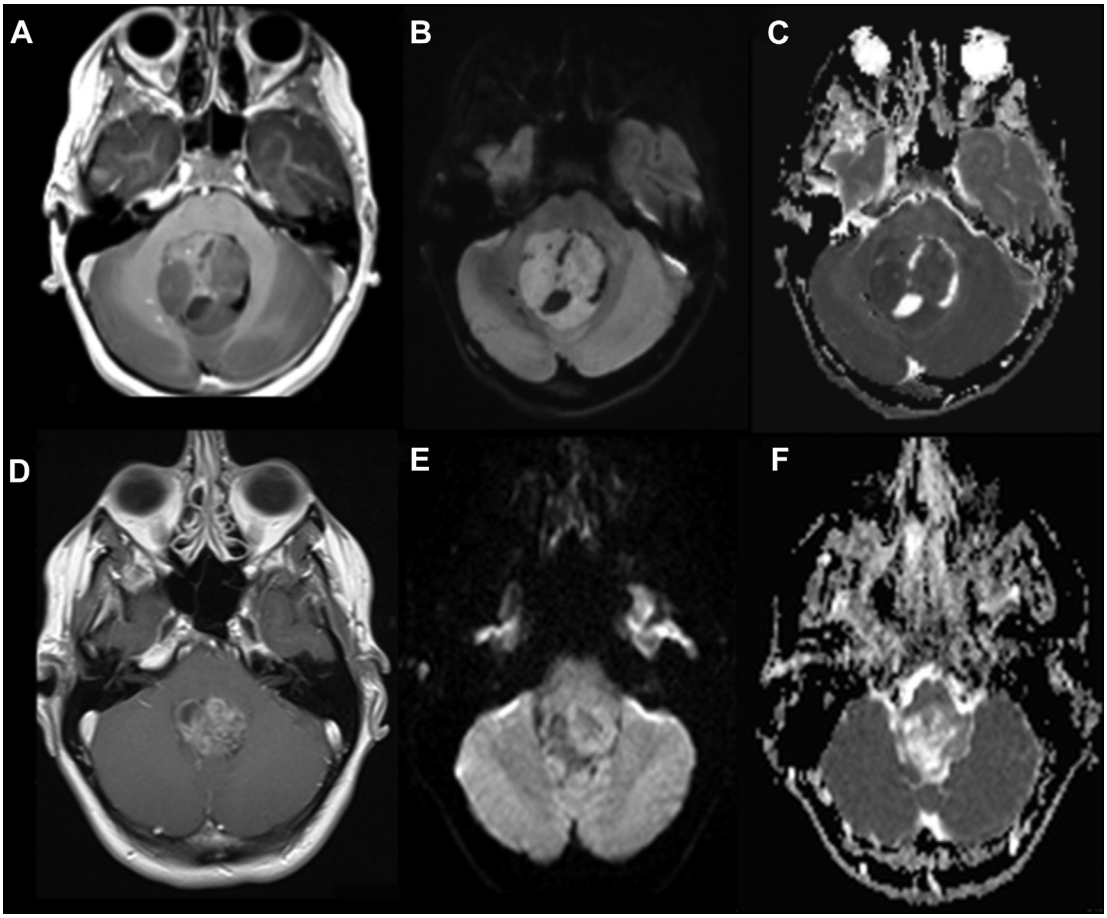

Fig. 1. Two different fourth ventricle tumors demonstrating heterogeneous enhancement on T1 postcontrast images. Medulloblastoma (*A*) demonstrating high signal intensity on DWI (*B*) and lower ADC than adjacent cerebellum (*C*). Ependymoma (*D*) demonstrating intermediate signal on DWI (*E*) but high ADC compared with the cerebellum (*F*).

low-grade gliomas (World Health Organization I and II).[10] Glioblastomas, in particular, are more heterogeneous than untreated lymphoma, with solid enhancing component demonstrating mild hyperintensity on DWI because of a combination of T2 shine-through and intermediate diffusion, and necrotic components demonstrating facilitated diffusion. Intratumoral hemorrhage is also more common in glioblastoma, and its associated susceptibility artifact can produce erroneous high DWI signal that must be recognized to avoid misinterpretation.

Other central nervous system tumors, especially those in the category of "small-blue-round-cell" tumors, such as primitive neuroectodermal tumor, germ cell tumor, and retinoblastoma, can demonstrate restricted diffusion. These are rarer and their characteristic locations can often provide helpful clues. Metastatic brain tumors can have variable appearance on DWI, depending on their primary source. Some have reported that the peritumoral edema of metastatic lesions have higher ADC than the nonenhancing component of gliomas, presumably because of higher cellularity of the latter.[11]

Nonneoplastic processes, such intracranial abscess and tumefactive demyelination, can often mimic tumor and demonstrate restricted diffusion. In contrast to lymphoma and other tumors, however, it is the central necrotic component of the abscess that demonstrates intense restricted diffusion rather than the solid cellular portion. Intracranial abscesses also tend to have relevant history and laboratory findings that aid in diagnosis. However, tumefactive demyelination can pose a diagnostic dilemma and appear similar to brain tumors, but its diffusion restriction is often along a "front" of active demyelination, occurring in a characteristic incomplete rim rather than a solid mass (**Fig. 2**).

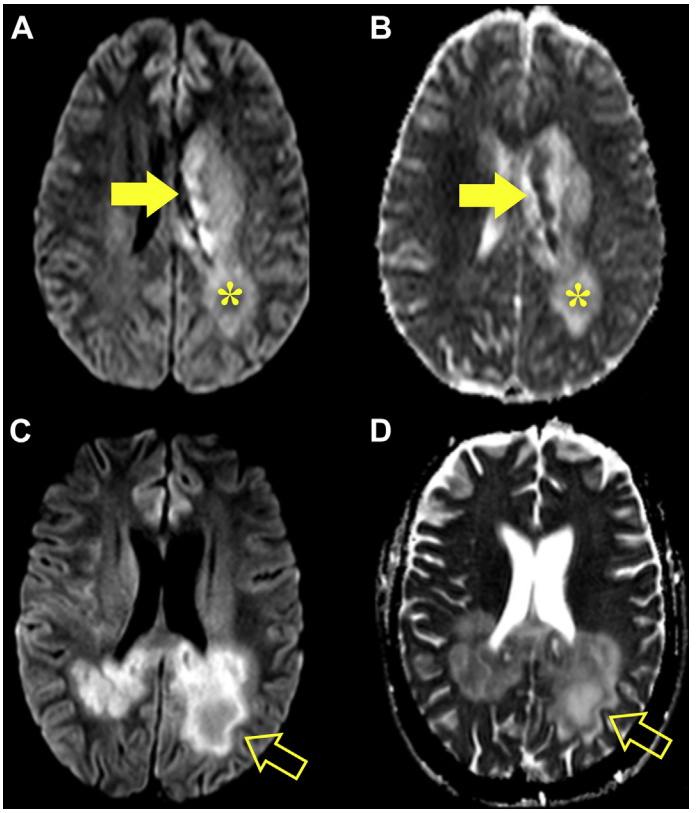

Fig. 2. Central nervous system lymphoma with foci of restricted diffusion (*arrows*) as shown on DWI (*A*) and ADC (*B*) along the left caudate and splenium, and extensive surrounding edema that demonstrates T2 shine-through (*asterisks*). (*C*, *D*) Tumefactive demyelination involving the splenium and periventricular white matter, with a thin rim of restricted diffusion along a front of active demyelination (*arrows*). Note the relative paucity of surrounding edema and mass effect despite a larger lesion in the case of tumefactive demyelination.

Post-treatment

A challenge in post-treatment imaging of brain tumors is the differentiation of treatment effects, from true tumor progression. Diffusion imaging can play a helpful role in this task when interpreted with detailed knowledge of tumor type and treatment history. In the immediate postsurgical setting, devitalized tissue along the resection cavity is expected to demonstrate restricted diffusion. Sometimes, however, the extent of restricted diffusion can extend beyond the surgical cavity and may involve large vascular territories, raising concern for perioperative infarction. This is more common when the mass is close to or encases vital vascular structures. Susceptibility artifact associated with postsurgical blood products can produce apparent hyperintensity on DWI and must be differentiated from true restricted diffusion.

Radiation therapy induces complex changes to the tumor and surrounding brain, which is dependent on tumor genetics, radiation dose, concurrent chemotherapy, and time. Paradoxic worsening of conventional image findings (enhancement and FLAIR) can occur within the first 3 months of completion of chemoradiation of high-grade gliomas, especially among tumors with IDH-1 mutation and methylation of the MGMT promoter.[12] This phenomenon is termed pseudoprogression and reflects an inflammatory response to tumor necrosis and connotes improved survival. A retrospective series evaluated the role of ADC ratio (minimal ADC in lesion/contralateral normal-appearing white matter) in differentiation between pseudoprogression and true progression, and found diagnostic accuracy of 86.7% when using ADC ratio alone, and 93.3% when used in a multiparametric model combined with dynamic susceptibility contrast perfusion and MR spectroscopy.[13] Interval increase in ADC after stereotactic radiosurgery of brain metastases has also been shown to be predictive of pseudoprogression, with accuracy of 77% according to one report.[14]

Radiation necrosis commonly occurs 3 months to a year following radiation and may be delayed for up to multiple years. Differentiation of radiation necrosis and tumor progression is difficult based on conventional imaging appearance, and addition of DWI has been shown to improve diagnostic accuracy. A recent study showed that addition of ADC cutoff of 1×10^{-3} mm^2/s to Brain Tumor Reporting and Data System improved its

diagnostic performance either alone (area under the curve, 0.76–0.88), or in combination with dynamic susceptibility contrast (area under the curve, 0.92).[15] Complex techniques that consider heterogeneity within a lesion, such as volume-weighted voxel-based multiparametric clustering of diffusion and perfusion features, improved diagnostic accuracy over single imaging parameters.[16] With the growth of machine learning and radiomics, there will undoubtedly be newer algorithms that incorporate conventional and advanced imaging features to classify tumor outcome. However, heterogeneity within treated tumor itself, where radiation necrosis often coexists with viable tumor, poses a challenge to the development and implementation of automated techniques.

The vascular endothelial growth factor inhibitor bevacizumab is commonly used in recurrent glioblastoma. This medication has antiangiogenic effects and reduces blood-brain barrier permeability, thereby masking the enhancement of viable tumor (pseudoresponse). Restricted diffusion can occur in either the tumor bed or elsewhere in the brain, presumably caused by ischemic necrosis (**Fig. 3**). Restricted diffusion in malignant gliomas treated with bevacizumab that is persistent over time is usually associated with good outcomes.[17] However, pathologic studies have shown that progressive bevacizumab-induced restricted diffusion is associated with coagulative necrosis surrounded by viable tumor and associated with poor outcomes.[18] Thus, it is important to evaluate serial changes in diffusion restriction on follow-up imaging and to incorporate all clinical and imaging data available to make the most accurate assessment.

DIFFUSION TENSOR IMAGING

Pretreatment

To preserve functional tissue, state-of-the-art MR imaging preoperative mapping of brain tumor patients has become the standard of care across the country. Neuroradiology-generated preoperative mapping of eloquent white matter tracts helps the neurosurgeon balance morbidity with resecting as much tumor as possible, which correlates with improved patient survival.[19] The emergence of DTI with FT has allowed neurosurgeons to resect tumors with decreased complication rates[20,21] and increased median survival rates.[22]

Knowledge of the technical basis of DTI combined with white matter anatomy is essential in the application of preoperative FT. DTI uses the

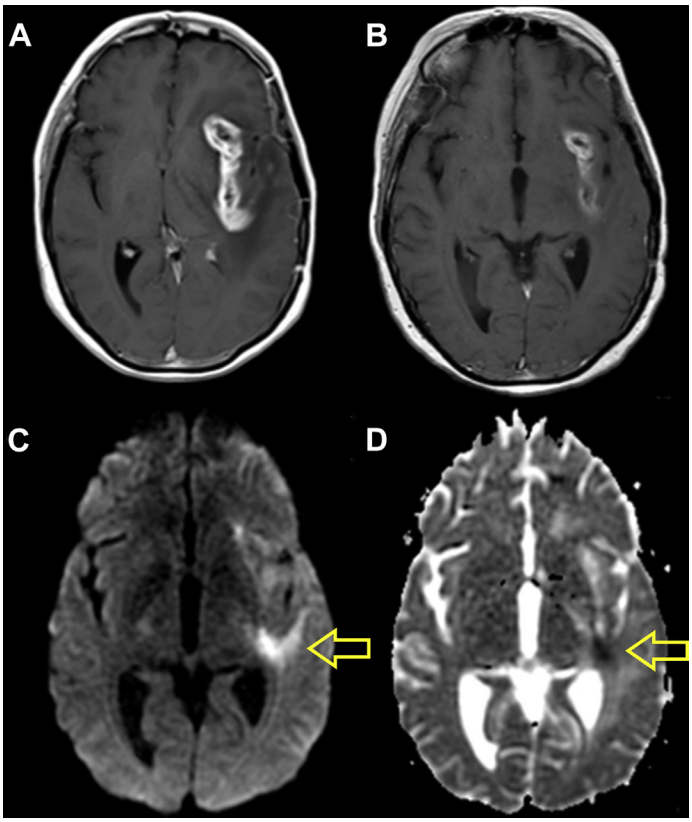

Fig. 3. Glioblastoma treated with bevacizumab demonstrating reduction of enhancement on pretreatment (*A*) and follow-up (*B*) T1 postcontrast images. Follow-up DWI (*C*) and ADC (*D*) shows diffusion restriction in the left temporal stem in the region of previous enhancement (*arrows*), corresponding to ischemic necrosis. Attention to this area on follow-up diffusion imaging is needed to assess for continued tumor response.

anisotropic diffusion of water along coherently organized white matter tracts. FA value of 1 means that diffusion happens along one axis and is restricted in other directions (ie, axonal bundle). Most clinical DTI protocols use at least 30 diffusion-encoded image sets at b = 1000 s/mm^2 along noncollinear directions in addition to b = 0 s/mm^2 image set with 2- to 3-mm isotropic voxels to create the diffusion tensor. Deterministic FT generates streamlines, originating from user-defined seed points, along the dominant diffusion direction of the tract in three-dimension (3D) from voxel to voxel. Tracking parameters can then be manipulated to constrain the streamlines to anatomically represent eloquent white matter pathways. Various technical aspects of FT have been discussed previously and are an essential review for anyone new to brain mapping.[23–26]

FT data are coregistered with volumetric structural sequences using various Food and Drug Administration–approved post-processing software for surgical navigation. The "buttonology" of these platforms varies, but the concepts of seed placement and tract titration are consistent. For nonenhancing tumors, it is paramount to fuse the tensor data with a 3D-FLAIR or T2 sequence. For enhancing lesions, postcontrast 3D-T1 images should be included. Seeds are placed in the plane perpendicular to the known trajectory of the desired tract to obtain as many streamlines as possible. A seed point can be drawn on several adjacent slices as another method to capture more streamlines. Our review focuses on two white matter tracts most frequently requested by our neurosurgical colleagues (corticospinal tract [CST] and arcuate fasciculus [AF]). Using real examples, we describe relevant anatomy, seed placement, and appropriate tract titration. A brief discussion on the limitations of clinical deterministic FT is included.

Motor: corticospinal tract

The CST or pyramidal tract is responsible for controlling movement in the contralateral torso, upper and lower extremities. It descends from the precentral gyrus and converges through the posterior limb internal capsule before traversing the brainstem.[26] It decussates at the caudal medulla and connects with spinal motor neurons. Using the direction-encoded color FA maps as a guide, the first seed is drawn in the axial plane to cover the cerebral peduncle (**Fig. 4**A). Cover as much of the peduncle as possible to ensure obtaining the CST fibers. The purpose of the second seed

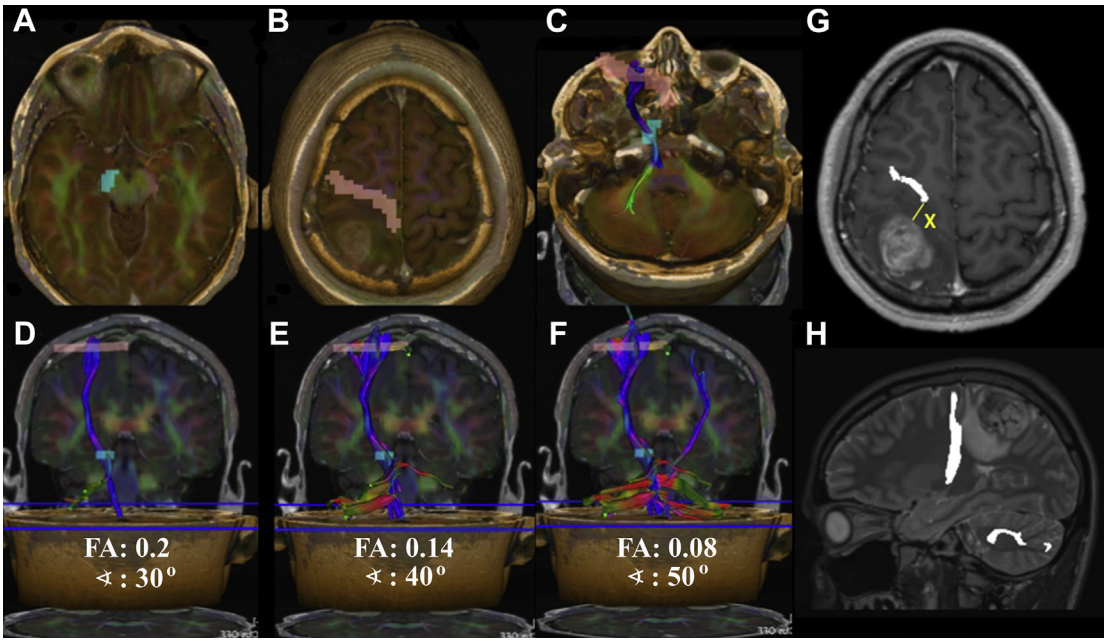

Fig. 4. Step-by-step CST tractography for a right parietal pleomorphic xanthoastrocytoma. (*A*, *B*) Axial 3D-T1 postcontrast images fused with direction-encoded color FA maps show the locations for seed placement: cerebral peduncle (*blue*) and precentral gyrus (*pink*). (*C*) Oblique axial image shows inclusion of streamlines only within both seed points. (*D–F*) Coronal images with different titration thresholds show sparse, appropriate, and excessive streamlines, respectively. (*G*) Axial 3D-T1 postcontrast and (*H*) sagittal 3D-T2 surgical navigation images show the 3D "burned-in" tract volume X mm from the enhancing tumor margin and along the nonenhancing signal abnormality.

point is to constrain the tract to match known anatomy.[27] The second seed is placed on axial images to cover the precentral gyrus subcortical white matter just inferior to the level of the hand knob (Fig. 4B). In the case of the CST the second seed point excludes the frontal pontine and parietal pontine fibers (Fig. 4C).

After the initial tract is generated, we then titrate our tract parameters to enhance the tract density while at the same time minimizing spurious fibers. An excellent review of CST parameter titration by Parizel and colleagues[28] provides suggested values. Fig. 4D–F shows examples of sparse, sufficient and excessive streamlines. A summary of parameters altering fiber tracking is found in Table 2. We report the smallest distance from the lesion's enhancing and nonenhancing margins relative to the visualized tract (Fig. 4G, H). Although this is not a universally accepted DTI practice because of the deterministic tractography limitations that are discussed later,[29] acknowledgment by surgeons that the tracts are estimated representations of white matter makes this a nonissue.

Language: arcuate fasciculus

The AF has been classically represented as the connection between the putative Broca and Wernicke language areas. Recent models of language connectivity in human cadaver[30] and DTI studies[31,32] favor the AF consisting of multiple complex components including indirect semantic and direct phonetic pathways. The AF extends from the caudal aspect of the superior and middle temporal gyri around the sylvian fissure and to the ipsilateral dorsal prefrontal cortex. To virtually dissect the AF, we place an initial seed on the direction-encoded color FA maps in the proximal frontal projections in the coronal plane at the level of the isthmus of the corpus callosum (Fig. 5A). The second seed is placed in the genu of the AF in the axial plane at the level of the internal capsule (Fig. 5B). When titrating, a higher angle threshold (60°–80°) should be used to overcome the curved portion of the tract.

Most humans have left language lateralization and the left AF is typically larger (Fig. 5D, E).[33,34] It has been theorized that the left AF may play an additional role in acoustic processing and will be larger even in right language lateralized subjects.[35] However, the right or nondominant AF should not be regarded as trivial because it contributes to prosody.[36] In left-handed and ambidextrous patients that tend to have bilateral hemisphere contributions to speech, use caution if relying on tractography of the AF without functional MR imaging task data to predict language lateralization, because there can be less AF asymmetry.[34,37] Correlating the bilateral AF tractography pattern with the Edinburgh Handedness Inventory score[38] is essential for right-sided lesion cases for best representation of the tracts.[34] The putative Wernicke area has a greater variability in location compared with Broca area.[39] In cases of suspected atypical language center localization, fusing the FT data to the functional MR imaging task data can increase reporting confidence if the data sets have common areas of involvement (Fig. 6).

Challenges and limitations

Neuroradiologists need to understand the limitations of tractography, such as patient motion, signal noise, magnetic field geometric distortions, and eddy-current artifacts. Neurosurgeons need to know that once the craniotomy is performed and debulking occurs, the brain shifts and the 3D tracts loaded to the navigation software may no longer align with the patient.[40] Another major limitation to the deterministic tensor model is the

Table 2
Summary of post-processing fiber tracking parameters and suggested starting values for tract titration

Parameter[a]	Increasing Parameter Effect on Fiber Density	Suggested Starting Value	
		CST	AF
FA threshold	Decreases	0.16	0.12
Angle threshold	Increases	40°	60°
Step length	Decreases	1.5 mm	1.5 mm
Samples per voxel length	Increases	2	3

FA threshold: fiber tracking will stop if FA is smaller than this value. Angle threshold: fiber tracking will stop if turning angle is larger than this value. Step length: for the streamline marching algorithm; should be about one-quarter of the voxel size. If too small will cause much longer tracking time with little increase in accuracy. Samples per voxel length: sample rate for user-defined seed region. Values larger than 4 may cause errors.

[a] Not all parameters are available to manually adjust on different software platforms.

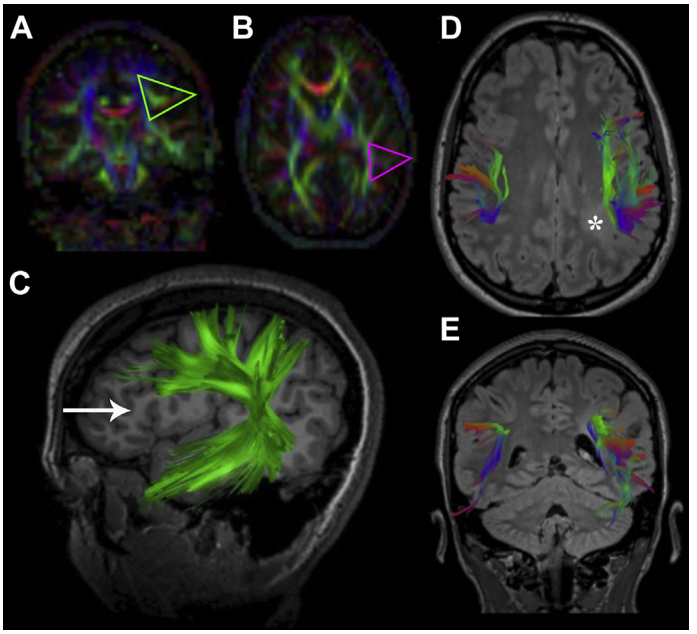

Fig. 5. (*A*, *B*) Coronal and axial direction-encoded color FA maps show the typical locations for seed placement for generating the left AF in a volunteer: periventricular *green triangle* and genu *purple triangle*. (*C*) Sagittal 3D-T1 image shows only streamlines included in both seed points. Note the lack of frontal fibers to the Broca area (*arrow*). (*D*, *E*) Axial and coronal 3D-FLAIR images with fused bilateral AF tracts show expected asymmetry in a right-handed (Edinburgh Handedness +100) individual with an infiltrative left parietal lesion (*asterisk*).

inability to resolve multiple fiber orientations within the imaging voxel.[41,42] This is known as the "crossing fiber problem." The estimate of tensor orientation is an average of the orientations of all the axons contained within the voxel. When the axons are coherently organized the tensor orientation reflects the underlying fibers. When the axons are not highly coherent, the voxel-averaged estimate of tensor orientation is not accurate and the tract stops prematurely or can continue spuriously. Although this issue is improved with higher angular resolution diffusion acquisitions[43] and probabilistic tractography,[44] voxels containing multiple-fiber orientations are likely whenever the imaging resolution (2–3 mm) is larger than the axon dimensions (several microns).

The lateral projections of the CST and the corticobulbar tracts (movement of the face and tongue) are notoriously nonvisualized because of crossing the lateral aspect of the AF while entering the corona radiata (**Fig. 7**).[44,45] Routinely when generating the AF, the anterior component to Broca area is truncated for unknown reasons (**Fig. 5**C). This may be caused by crossing short frontal tracts

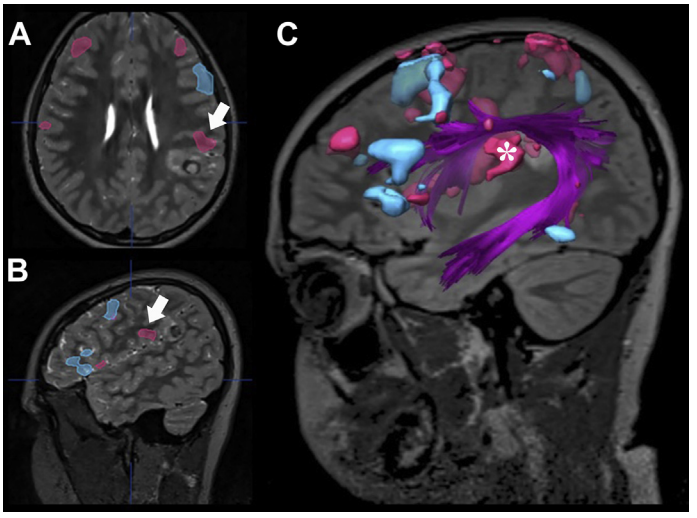

Fig. 6. Superimposing the DTI data to the functional MR imaging task data can increase confidence in mapping atypical language centers. (*A*, *B*) Axial and sagittal 3D-T2 images with coregistered verb generation (*blue*) and semantic decision (*red*) tasks for a left parietal extraventricular neurocytoma. There is a dominant receptive language center (*arrows*) in an atypical location in the supramarginal gyrus. Activity was not seen in the classic Wernicke location of posterior superior temporal gyrus. (*C*) 3D-FLAIR fused with left AF volume (*purple*) shows the streamlines involving the receptive language center (*asterisk*) increasing confidence. There was impairment of phonologic retrieval during intraoperative cortical stimulation of this center.

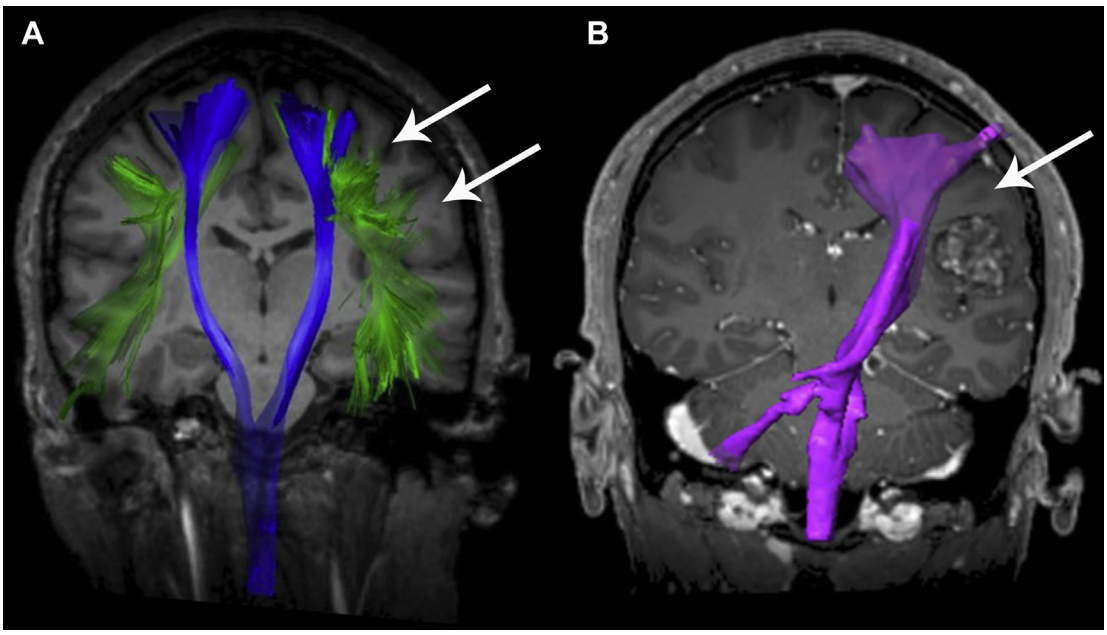

Fig. 7. (*A*) Coronal 3D-T1 fused with bilateral CST (*blue*) and AF (*green*) tracts in a volunteer shows the location of missing lateral CST and corticobulbar streamlines (*arrows*) from crossing fibers. (*B*) Coronal 3D-T1 postcontrast of a patient with a cavernoma shows missing lateral streamlines of the CST (*purple*) over the superior aspect of the lesion (*arrow*). It is important to report expected locations of nonvisualized fibers before surgery.

including the frontal aslant pathway.[46] An electrocorticography study combined with DTI of the AF found that language-related sites in the temporal lobe were far more likely to directly connect to the inferior precentral gyrus rather than Broca area.[47] This may suggest the AF plays a supporting role and interacts with other language tracts that have a direct connection to Broca area. Using knowledge of white matter anatomy one can anticipate where these classically "missing" fiber components would be relative to the lesion and inform the neurosurgeon in their report.

Absence of fibers may also occur when there is extensive edema, tumor infiltration, or frank destruction. Delineation of the two latter scenarios is problematic because both may occur with the same lesion. New research tractography approaches are able to overcome the "edema problem."[48] Until they are ready for widespread clinical implementation, reducing the FA threshold to increase visualization of absent fibers remains an alternative, albeit not always successful. Tumor imaging patterns with tractography have been previously described.[26] In the case of frank destruction by tumor, a near zero anisotropy is seen and the tract is not visualized no matter the decrease in FA threshold. With tract infiltration by tumor, the tract is deviated into an abnormal orientation with an abnormally low FA. In cases of peritumoral edema there is an abnormally low FA but no deviation in tract orientation. These three patterns can each reduce FA, therefore one should not confuse FA values with white matter integrity. Observation of function during functional MR imaging training by the neuroradiologist or cortical activation with relevant tasks is superior to absence of DTI fibers (**Fig. 8**).

Post-treatment

Previous works have evaluated DTI as a means to predict functional recovery after surgery. They have evaluated distances and indirectly estimated axonal health via DTI metrics, such as FA and diffusivity. Lower FA averages and higher mean diffusivity in the ipsilateral CST have been linked to postoperative motor deficits.[49] FA values of interhemispheric connectivity were associated with postoperative aphasia in left-sided perisylvian brain tumors.[50] A tumor distance of 1 cm or less from the CST or AF most significantly predicts the occurrence of new deficits with current surgical techniques.[51] Furthermore, an intraoperative subcortical motor stimulation study showed a 1-cm gap of uncertainty between the bipolar electrode tip and generated DTI tracts.[52] Therefore we favor clearly describing "impression worthy" tracts that are 1 cm or less from the tumor margins in our functional MR imaging reports. The DTI tractography plans can improve safety of surgery by

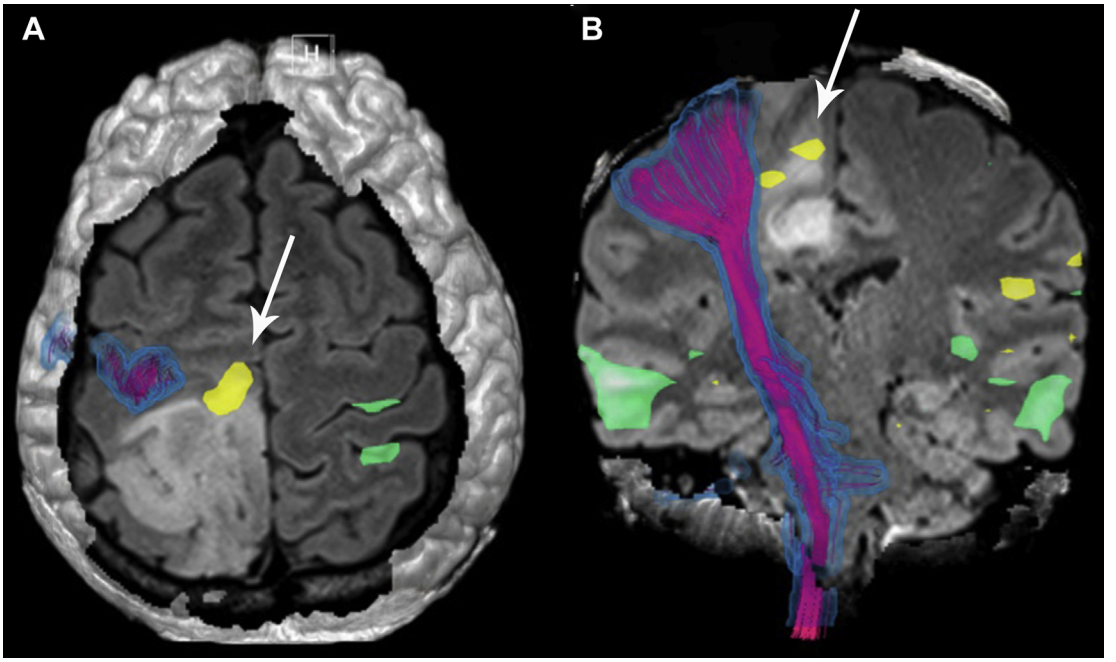

Fig. 8. (*A*) Axial and (*B*) coronal 3D-FLAIR images of a right parietal IDH-mutated glioma. The CST (*pink*) medial fibers to the leg/foot area of the right precentral gyrus are not visualized because of decreased FA from tumor infiltration. Foot motion was intact during patient training and superimposed functional MR imaging ankle flexion task data (*yellow*) show activity (*arrows*). Reporting the medial CST fibers are functioning even though not recognized by the tractography algorithm is crucial for surgical planning.

identifying challenging resection margins and informing the surgeons when to brace for a possible challenging postoperative recovery.

Diffusion tensor–derived quantitative measures can act as biomarkers for worsening disease in the absence of appreciable change on conventional MR imaging sequences. Restriction on DTI maps can detect low-grade glioma malignant transformation (axial diffusivity having highest sensitivity and specificity) at the same time point or earlier compared with contrast-enhanced images.[53] Significantly decreased FA at baseline in the glioma peritumoral nonenhancing signal abnormality is a predictor of local enhancing tumor recurrence.[54] These findings may be important for surgery or radiation planning. The toxic effects of chemoradiation therapy on cerebral white matter linked to cognitive changes are assessed with DTI. Connor and colleagues[55] showed mean, axial, and radial diffusivity significantly increased with radiation time course and dose and corresponding decrease in FA in white matter of high-grade glioma patients. They postulated the radiation-induced vascular permeability and neuroinflammation contributed to neurocognitive decline. The structural integrity of white matter is susceptible to the effects of chemotherapy. Medulloblastoma patients treated with chemotherapy had decreased FA values in white matter structures compared with healthy age-matched control subjects. Reductions in FA values were associated with poor performance at school.[56]

CLINICS CARE POINTS

- Reduced ADC values are seen in highly cellular brain tumors, such as lymphoma, medulloblastoma, and atypical meningioma.
- Progressive reduced diffusion over time is associated with poor outcomes in malignant gliomas treated with bevacizumab.
- The arcuate fasciculi typically have greater hemispheric asymmetry than the corticospinal tracts and should be correlated with Edinburgh Handedness score.
- Tumor infiltration and edema can reduce FA values to the point that functioning fiber tracts are not recognized by deterministic tractography.
- Document eloquent fiber tracts that are 1 cm or less from the tumor margin in the functional MR imaging report impression.

DISCLOSURES

The authors have nothing to disclose.

REFERENCES

1. Schaefer PW, Grant PE, Gonzalez RG. Diffusion-weighted MR imaging of the brain. Radiology 2000;217(2):331–45.
2. Kono K, Inoue Y, Nakayama K, et al. The role of diffusion-weighted imaging in patients with brain tumors. AJNR Am J Neuroradiol 2001;22(6):1081–8.
3. Holodny AI, Ollenschlager M. Diffusion imaging in brain tumors. Neuroimaging Clin N Am 2002;12(1):107–24.
4. Hygino da Cruz LC Jr, Vieira IG, Domingues RC. Diffusion MR imaging: an important tool in the assessment of brain tumors. Neuroimaging Clin N Am 2011;21(1):27–49.
5. Filippi CG, Edgar MA, Uluğ AM, et al. Appearance of meningiomas on diffusion-weighted images: correlating diffusion constants with histopathologic findings. AJNR Am J Neuroradiol 2001;22(1):65–72.
6. Shankar JJS, Hodgson L, Sinha N. Diffusion weighted imaging may help differentiate intracranial hemangiopericytoma from meningioma. J Neuroradiol 2019;46(4):263–7.
7. Tsuruda JS, Chew WM, Moseley ME, et al. Diffusion-weighted MR imaging of the brain: value of differentiating between extraaxial cysts and epidermoid tumors. AJNR Am J Neuroradiol 1990;11(5):925–31 [discussion: 932–4].
8. Rumboldt Z, Camacho DLA, Lake D, et al. Apparent diffusion coefficients for differentiation of cerebellar tumors in children. AJNR Am J Neuroradiol 2006;27(6):1362–9.
9. Toh C-H, Castillo M, Wong AM-C, et al. Primary cerebral lymphoma and glioblastoma multiforme: differences in diffusion characteristics evaluated with diffusion tensor imaging. AJNR Am J Neuroradiol 2007;29(3):471–5.
10. Hilario A, Ramos A, Perez-Nuñez A, et al. The added value of apparent diffusion coefficient to cerebral blood volume in the preoperative grading of diffuse gliomas. AJNR Am J Neuroradiol 2011;33(4):701–7.
11. Lee EJ, terBrugge K, Mikulis D, et al. Diagnostic value of peritumoral minimum apparent diffusion coefficient for differentiation of glioblastoma multiforme from solitary metastatic lesions. AJR Am J Roentgenol 2011;196:71–6.
12. Li H, Li J, Cheng G, et al. IDH mutation and MGMT promoter methylation are associated with the pseudoprogression and improved prognosis of glioblastoma multiforme patients who have undergone concurrent and adjuvant temozolomide-based chemoradiotherapy. Clin Neurol Neurosurg 2016;151:31–6.
13. Matsusue E, Fink JR, Rockhill JK, et al. Distinction between glioma progression and post-radiation change by combined physiologic MR imaging. Neuroradiology 2010;52(4):297–306.
14. Knitter JR, Erly WK, Stea BD, et al. Interval change in diffusion and perfusion MRI parameters for the assessment of pseudoprogression in cerebral metastases treated with stereotactic radiation. Am J Roentgenol 2018;211(1):168–75.
15. Yang Y, Yang Y, Wu X, et al. Adding DSC PWI and DWI to BT-RADS can help identify postoperative recurrence in patients with high-grade gliomas. J Neurooncol 2020;146(2):363–71.
16. Yoon RG, Kim HS, Koh MJ, et al. Differentiation of recurrent glioblastoma from delayed radiation necrosis by using voxel-based multiparametric analysis of MR imaging data. Radiology 2017;285(1):206–13.
17. Mong S, Ellingson BM, Nghiemphu PL, et al. Persistent diffusion-restricted lesions in bevacizumab-treated malignant gliomas are associated with improved survival compared with matched controls. AJNR Am J Neuroradiol 2012;33(9):1763–70.
18. Nguyen HS, Milbach N, Hurrell SL, et al. Progressing bevacizumab-induced diffusion restriction is associated with coagulative necrosis surrounded by viable tumor and decreased overall survival in patients with recurrent glioblastoma. AJNR Am J Neuroradiol 2016;37(12):2201–8.
19. Claus EB, Horlacher A, Hsu L, et al. Survival rates in patients with low-grade glioma after intraoperative magnetic resonance image guidance. Cancer 2005;103:1227–33.
20. Ulmer JL, Berman JI, Meuller WN, et al. Issues in translating imaging technology and presurgical diffusion tensor imaging. In: Faro SH, Mohamed FB, Law M, et al, editors. Functional neuroradiology: principles and clinical applications. 1st edition. Boston (MA): Springer; 2011. p. 731–65.
21. Bello L, Castellano A, Fava E, et al. Intraoperative use of diffusion tensor imaging fiber tractography and subcortical mapping for resection of gliomas: technical considerations. Neurosurg Focus 2010;28(2):E6.
22. Wu JS, Zhou LF, Tang WJ, et al. Clinical evaluation and follow-up outcome of diffusion tensor imaging-based functional neuronavigation: a prospective, controlled study in patients with gliomas involving pyramidal tracts. Neurosurgery 2007;61(5):935–48 [discussion: 948–9].
23. Mukherjee P, Berman JI, Chung SW, et al. Diffusion tensor MR imaging and fiber tractography: theoretic underpinnings. AJNR Am J Neuroradiol 2008;29:632–41.
24. Mukherjee P, Chung SW, Berman JI, et al. Diffusion tensor MR imaging and fiber tractography: technical

considerations. AJNR Am J Neuroradiol 2008;29:843–52.
25. Catani M, Howard RJ, Pajevic S, et al. Virtual in vivo interactive dissection of white matter fasciculi in the human brain. Neuroimage 2002;17:77–94.
26. Jellison BJ, Field AS, Medow J, et al. Diffusion tensor imaging of cerebral white matter: a pictorial review of physics, fiber tract anatomy, and tumor imaging patterns. AJNR Am J Neuroradiol 2004;25:356–69.
27. Carpenter MB, Strong OS, Truex RC. Human neuroanatomy: (formerly Strong and Elwyn's human neuroanatomy). 7th edition. Baltimore (MD): Lippincott Williams & Wilkins; 1976.
28. Parizel PM, Van Rompaey V, Van Loock R, et al. Influence of user-defined parameters on diffusion tensor tractography of the corticospinal tract. Neuroradiology J 2007;20:139–47.
29. Field A, Filippi C, Kalnin A, et al. ASFNR guidelines for clinical application of diffusion tensor imaging. 2012. Available at: www.asfnr.org/clinical-standards. Accessed April 21, 2020.
30. Dick AS, Tremblay P. Beyond the arcuate fasciculus: consensus and controversy in the connectional anatomy of language. Brain 2012;135:3529–50.
31. Catani M, Mesulam M. The arcuate fasciculus and the disconnection theme in language and aphasia: history and current state. Cortex 2008;44:953–61.
32. Glasser MF, Rilling JK. DTI tractography of the human brain's language pathways. Cereb Cortex 2008;18:2471–82.
33. Vernooij MW, Smits M, Wielopolski PA, et al. Fiber density asymmetry of the arcuate fasciculus in relation to functional hemispheric language lateralization in both right- and left-handed healthy subjects: a combined fMRI and DTI study. Neuroimage 2007;35(3):1064–76.
34. Propper RE, O'Donnell LJ, Whalen S, et al. A combined fMRI and DTI examination of functional language lateralization and arcuate fasciculus structure: effects of degree versus direction of hand preference. Brain Cogn 2010;73:85–92.
35. Hutsler J, Galuske RA. Hemispheric asymmetries in cerebral cortical networks. Trends Neurosci 2003;8:429–35.
36. Ethofer T, Anders S, Erb M, et al. Cerebral pathways in processing of affective prosody: a dynamic causal modeling study. Neuroimage 2006;30:580–7.
37. Szaflarski JP, Binder JR, Possing ET, et al. Language lateralization in left-handed and ambidextrous people: fMRI data. Neurology 2002;2:238–44.
38. Oldfield RC. The assessment and analysis of handedness: the Edinburgh inventory. Neuropsychologia 1971;9(1):97–113.
39. Chang EF, Raygor KP, Berger MS. Contemporary model of language organization: an overview for neurosurgeons. J Neurosurg 2015;122:250–61.
40. Nimsky C, Ganslandt O, Hastreiter P, et al. Preoperative and intraoperative diffusion tensor imaging-based fiber tracking in glioma surgery. Neurosurgery 2005;56(1):130–7 [discussion: 138].
41. Basser PJ, Mattiello J, Le Bihan D. Estimation of the effective self-diffusion tensor from the NMR spin echo. J Magn Reson 1994;103:247–54.
42. Pierpaoli C, Basser PJ. Toward a quantitative assessment of diffusion anisotropy. Magn Reson Med 1996;36:893–906.
43. Caverzasi E, Hervey-Jumper SL, Jordan KM, et al. Identifying preoperative language tracts and predicting postoperative functional recovery using HARDI q-ball fiber tractography in patients with gliomas. J Neurosurg 2015;125:33–45.
44. Behrens TEJ, Berg HJ, Jbabdi S, et al. Probabilistic diffusion tractography with multiple fibre orientations: what can we gain? Neuroimage 2007;34:144–55.
45. Holodny AI, Watts R, Korneinko VN, et al. Diffusion tensor tractography of the motor white matter tracts in man: current controversies and future directions. Ann N Y Acad Sci 2005;1064:88–97.
46. Catani M, Dell'Acqua F, Vergani F, et al. Short frontal lobe connections of the human brain. Cortex 2012;48:273–91.
47. Brown EC, Jeong JW, Muzik O, et al. Evaluating the arcuate fasciculus with combined diffusion weighted MRI tractography and electrocorticography. Hum Brain Mapp 2014;35(5):2333–47.
48. Zhang H, Wang Y, Lu T, et al. Differences between generalized q-sampling imaging and diffusion tensor imaging in the preoperative visualization of the nerve fiber tracts within peritumoral edema in brain. Neurosurgery 2013;73:1044–53 [discussion: 1053].
49. Rosenstock T, Giampiccolo D, Schneider H, et al. Specific DTI seeding and diffusivity-analysis improve the quality and prognostic value of TMS-based deterministic DTI of the pyramidal tract. Neuroimage Clin 2017;16:276–85.
50. Sollmann N, Negwer C, Tussis L, et al. Interhemispheric connectivity revealed by diffusion tensor imaging fiber tracking derived from navigated transcranial magnetic stimulation maps as a sign of language function at risk in patients with brain tumors. J Neurosurg 2016;126:222–33.
51. Meyer EJ, Gaggl W, Gilloon B, et al. The impact of intracranial tumor proximity to white matter tracts on morbidity and mortality: a retrospective diffusion tensor imaging study. Neurosurgery 2017;80:193–200.
52. Berman JI, Berger MS, Chung SW, et al. Accuracy of diffusion tensor magnetic resonance imaging tractography assessed using intraoperative subcortical stimulation mapping and magnetic source imaging. J Neurosurg 2007;107(3):488–94.

53. Freitag MT, Maier-Hein KH, Binczyk F, et al. Early detection of malignant transformation in resected WHO II low-grade glioma using diffusion tensor-derived quantitative measures. PLoS One 2016; 11(10):e0164679.
54. Bette S, Huber T, Gempt J, et al. Local fractional anisotropy is reduced in areas with tumor recurrence in glioblastoma. Radiology 2017;283(2):499–507.
55. Connor M, Karunamuni R, McDonald C, et al. Dose-dependent white matter damage after brain radiotherapy. Radiother Oncol 2016;121(2):209–16.
56. Khong PL, Kwong DLW, Chan GCF, et al. Diffusion-tensor imaging for the detection and quantification of treatment-induced white matter injury in children with medulloblastoma: a pilot study. AJNR Am J Neuroradiol 2003;24(4):734–40.